Inorganic Chemistry

ARTICLE

pubs.acs.org/IC

Directly Assembling Ligand-Free ZnO Nanocrystals into Three-Dimensional Mesoporous Structures by Oriented Attachment

Yunxin Liu, Dingsheng Wang, Qing Peng,* Deren Chu, Xiangwen Liu, and Yadong Li

Department of Chemistry, Tsinghua University, Beijing 100084, China

Supporting Information

ABSTRACT: Mesoporous materials have found a great number of important utilities due to their well-defined pore structure and high internal surface area, which are routinely synthesized with the assistance of block copolymers or templates. So far, a key challenge is how to assemble directly ligand-free inorganic nanocrystals into mesoporous structures, so that the high surface activity of ligand-free nanocrystals is not destroyed by further treatment to remove organic species or templates. In this paper, we report the direct assembly of highly uniform ZnO mesoporous ellipsoids from ligand-free ZnO nanocrystals of ~5 nm. The size of the synthesized uniform ZnO mesoporous ellipsoids can be efficiently tuned from 132 × 75 to 190 × 111 nm (length × width), by varying the size and concentration of primary ZnO nanocrystal building blocks and the composition of the designed assembling solvent. The BET detection indicates that these ZnO mesoporous ellipsoids have high specific surface areas reaching to 136.57 m^2/g, while their average BJH pore diameters are located at 8.8 nm. Especially, the high-resolution TEM images and XRD analysis revealed the occurrence of an oriented attachment mechanism in the assembly of uniform ZnO mesoporous ellipsoids, which supplied an important proof for the possibility of constructing stable three-dimensional structures by oriented attachment. The benefits of these ZnO mesoporous ellipsoids were demonstrated by their excellent photocatalytic activity under weak UV irradiation.

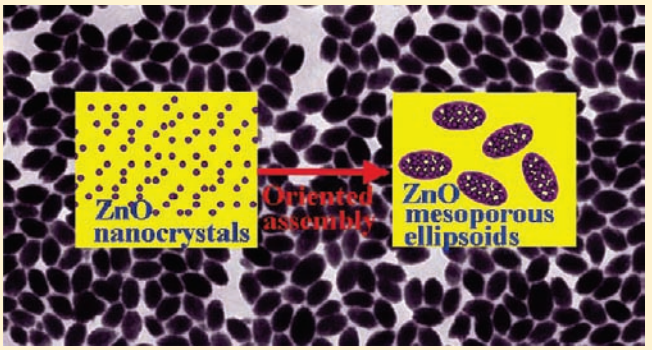

1. INTRODUCTION

Since their remarkable features were described in 1992, mesoporous materials (2 nm < pore size < 50 nm) have received increasing attention and been intensively studied with regard to applications in the fields of catalysis, biological engineering, and photoelectronic devices.[1−8] Many procedures have been designed to synthesize inorganic mesoporous materials with desirable physical and chemical properties.[8−16] Generally, the most popular method for mesoporous materials focused on the approach with the assistance of block copolymer; e.g., Zhao et al. reported triblock copolymer directed syntheses of mesoporous silica with periodic 5−30 nm pores, in which the block copolymer species can be recovered for reuse by solvent extraction or removed by heating.[12] Another well-known strategy is based on metal−organic frameworks constructed from molecular building blocks, by which two (2D) or three-dimensional (3D) pore sizes and structures can be designed and fabricated using various molecular struts.[17−19]

Recently, our group has developed a general emulsion-based bottom-up self-assembly (EBS) approach for assembling various kinds of ligand-stabilized nanocrystal building blocks into 3D colloidal spheres with mesoporous characteristics in which an organic ligand plays a key role for the successful assembly of 3D microstructures.[20−24]

These reported methods usually involved the elimination of organic groups or templates, in which some intrinsic problems needed to be carefully resolved, e.g., organic residual, surface activity lowering of nanocystalline walls in the calcination of organic groups, and interface reaction between mesoporous materials and templates. It is very attractive and desirable to design a novel procedure so that the ligand-free inorganic nanocrystals can be used to directly assemble the stable mesoporous structures at room temperature, in which no organic groups and templates need to be removed. However, it is very hard to control the dynamic behavior of ligand free nanocrystals, since they tend to agglomerate. Therefore, a key challenge is how to control the assembling dynamics of ligand-free nanocrystals so that the expected structures are obtained instead of a fast and irregular agglomeration.

In this work, we designed an efficient procedure to control the nucleation and growth dynamics in the assembling process so that ligand-free ZnO nanocrystals could be directly assembled into 3D mesoporous ellipsoids by oriented attachment (OA), in which the high surface activity of ligand-free nanocrystals is well-reserved. Equally important, our results indicate that the limitation to the 3D assembly by OA mechanism can be overcome by

Received: April 28, 2011
Published: May 24, 2011

controlling properly the viscosity and potential barrier of the solvent. The benefits of these ZnO mesoporous ellipsoids are confirmed by the excellent photocatalytic activity under weak UV irradiation.

2. EXPERIMENTAL SECTION

2.1. Synthesis of ZnO Nanocrystals. Zinc acetate dihydrate was first dissolved in methanol with Zn^{2+} concentration of 0.1 mol/L. Then, another solution was prepared by dissolving potassium hydroxide in methanol with an OH^- concentration of 3.4 mol/L. Under vigorous stirring, the potassium hydroxide solution was added dropwise to the zinc acetate solution with a Zn^{2+}/OH^- ratio of 1/1.7 at a temperature of 55 °C. After the addition of potassium hydroxide, the solution was evaporated at a rate of 1 mL/min. After being evaporated to be half of its initial volume, the solution was capped and kept heating and stirring until the total reaction time reached 2 h and 15 min. Finally, the solution was allowed to cool to room temperature, and white ZnO nanocrystals without organic ligand were produced.[25]

2.2. Assembly of ZnO Mesoporous Ellipsoids. The solvent system was prepared by mixing methanol/diethyl carbonate/chloroform (MDC) with volume ratio of 50/1.5/25. Then, the above stocked ZnO nanocrystal solutions was poured into the MDC solvent system with ZnO concentration of 4.2 mg/mL, to form a homogeneous solution system due to the good dispersity of the synthesized ZnO nanocrystals in methanol and chloroform. The homogeneous solution was further aged for 3 days, and highly uniform ZnO mesoporous ellipsoids were generated. For preparing Ag/ZnO mesoporous ellipsoid heterostructures, ZnO mesoporous ellipsoids were washed with methanol and dried at the temperature of 60 °C for 12 h. Then, 60 mg of the dried ZnO mesoporous ellipsoids was dispersed in 50 mL of distilled water with magnetic stirring. Subsequently, 10 mL of $AgNO_3$ aqueous solution (Ag^+ 0.0022 mmol/mL) was added dropwise and the solution was kept stirring at 50 °C for 1 h. After being removed from the heater and stirrer, the solution was kept stationary for another 1 h. Finally, the Ag−ZnO heterostructures were successfully produced.

2.3. Characterization. The morphology of the synthesized samples was measured using a Hitachi model H-800 and JEOL 2010 transmission electron microscope and a JEOL JSM-6301F scanning electron microscope. High-resolution TEM (HRTEM) measurements were performed by using a FEI Tecnai G2 F20 S-Twin electron microscope with an acceleration voltage of 200 kV. Powder X-ray diffraction patterns were recorded with a Bruker D8 Advance X-ray powder diffractometer with Cu Kα radiation (λ = 1.5406 Å). BET surface areas and Barret−Joyner−Halenda (BJH) pore-size distributions were measured with N^2 at 77 K by using a Quantachrome Autosorb-1 instrument.

2.4. Photocatalysis. Before the photocatalytic measurement, ZnO mesoporous ellipsoids or Ag/ZnO mesoporous ellipsoids were washed with methanol and dried at 60 °C for 12 h. Methylene blue (MB) was employed as a model dye to evaluate the photocatalytic activity of the uniform ZnO mesoporous ellipsoids. For photocatalytic measurement, 20 mg of ZnO mesoporous ellipsoids or 24 mg of Ag/ZnO mesoporous ellipsoids was dispersed in 80 mL of 10 ppm MB aqueous solution. The photocatalytic reaction was conducted at room temperature under weak UV irradiation (365 nm, 2.1 mW/cm^2), among which the reaction solution was slowly stirred with a magnetic stirrer to ensure full suspension of the particles throughout the experiment. Each experiment was conducted for 40 min with 3 mL sample aliquots extracted every 10 min. The decomposition of MB was monitored by measuring the absorbance of the aliquot solution using an UV−vis spectrophotometer with deionized water as reference.

3. RESULTS AND DISCUSSION

3.1. Assembling Processes and Principles. Inspired by previous works,[26−29] we predict that it is possible to control the dynamic process of nanocrystal building blocks in assembly process, if the solvent system is properly selected with suitable viscosity and potential barrier. For the direct assembly of uniform ZnO mesoporous ellipsoids, we try to control the moving speed, frequency, and direction of ligand-free ZnO nanocrystal building blocks by designing a MDC solvent system with suitable viscosity and potential barrier. It should be first declared that the synthesized ZnO nanocrystals in this work can dissolve in methanol and chloroform, but not in diethyl carbonate. Thus, the synthesized ZnO nanocrystals can move freely in methanol/chloroform if diethyl carbonate is not added. However, a potential barrier will arise in the solvent system after the addition of diethyl carbonate, which affects evidently the collision process of ZnO nanocrystals according to the collision theory, where the coalescence between nanocrystals may take place.[26] In other words, for ZnO nanocrystal assembly, the potential barrier of the designed MDC solvent system can be efficiently adjusted by varying the concentration of diethyl carbonate. On the other hand, the addition of diethyl carbonate can also change remarkably the viscosity of the whole solvent system, since the viscosity (0.75) of diethyl carbonate is obviously higher than those (0.58 and 0.57) of methanol and chloroform. Thereby, it can be concluded that the adjustment of diethyl carbonate content could supply the assembly of ZnO nanocryatals with suitable viscosity and potential barrier, if the concentration of methanol and chloroform is properly fixed prior to the addition of diethyl carbonate.

In the reported assembly of CuO ellipsoids, it has been demonstrated that weakly protected nanoparticles often undergo entropy-driven aggregation through strong interactions between the particles themselves.[30−32] The aggregation driving force along different axis depends on the atomic density of the corresponding crystal planes. In the case of this paper, the ligand-free ZnO nanocrystals undergo a similar oriented aggregation process, although the solution system may play a different assistant role for OA. Ostwald ripening and recrystallization should not occur in the assembly of ZnO mesoporous ellipsoids,

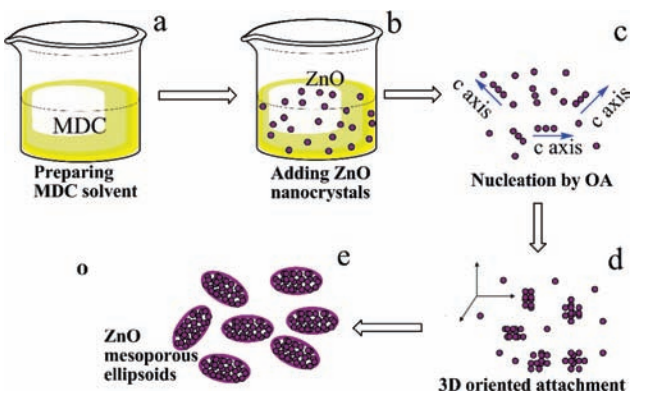

Figure 1. Assembly mechanism of ZnO mesoporous ellipsoids by OA: (a) the MDC solvent was prepared, (b) ZnO nanocrystals were added into the MDC solvent, (c) numerous nuclei were generated with the coalescence of several ZnO nanoparticles along the *c* axis, (d) the 3D assembly occurred by OA upon extending the aging time, and (e) the final ZnO mesoporous ellipsoids were produced after aging for 3 days.

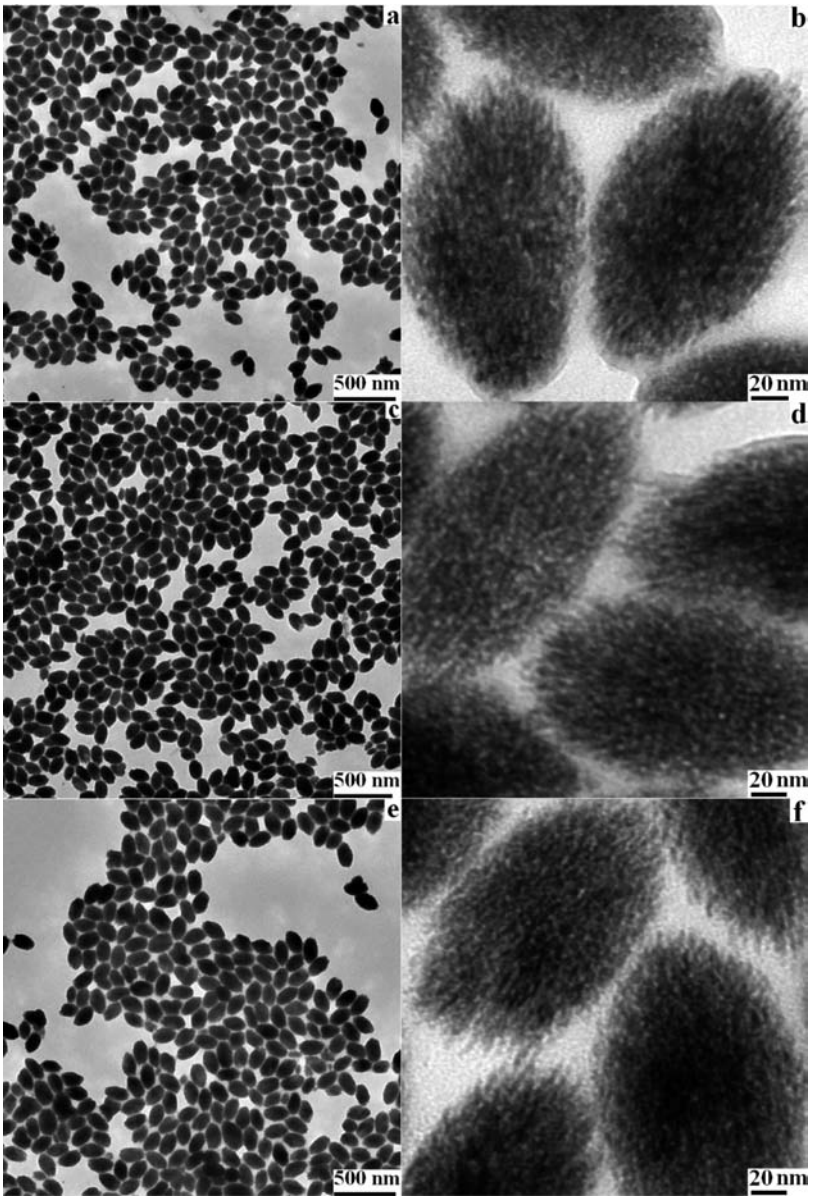

Figure 2. TEM images of highly uniform ZnO mesoporous ellipsoids assembled from 5 nm ZnO nanocrystals. (a, b) TEM images with different magnifications of uniform ZnO mesoporous ellipsoids with length× width of 175 × 101 nm, synthesized with 2 vol % of hexane added in MDC solvent. (c, d) length × width of 183 × 106 nm, synthesized with 1 vol % of hexane added in MDC solvent. (e, f) length × width of 190 × 111 nm, synthesized without hexane added in MDC solvent.

since the complete elimination of the surfaces and dissolution of primary ZnO nanocrystals have not been obviously observed.

Prior to the assembly of ZnO mesoporous ellipsoids, primary ZnO nanocrystals with the diameter of ~5 nm, shown in Figure S1 (Supporting Information), were produced as reported.[25] The basic assembling process and principles of highly uniform ZnO mesoporous ellipsoids in the MDC solvent system are specifically illustrated in Figure 1. First, a homogeneous solvent system containing methanol, chloroform, and diethyl carbonate was easily prepared due to the good compatibility among them. After adding of the as-synthesized ZnO nanocrystals into the solvent system, aggregation of ZnO nanocrystal building blocks will occur immediately, which produces numerous nuclei composed of several ZnO nanocrystal building blocks along the *c* axis. With aging time extended, the nuclei grew gradually by the OA of ZnO nanocrystal building blocks both along and perpendicular to the *c* axis due to the impact of the viscosity and potential barrier. After aging for enough time, all of the ZnO nanocrystal building blocks were consumed, so that the final mesoporous ellipsoids formed with almost perfect crystallographic orientations. In previously reported 1D assembly by OA,[25,28,29,33,34] the assembling dynamics might be mainly governed by the viscosity of solvent. Differentially, the importance of the potential barrier should be boosted in the 3D assembly by OA. We will demonstrate how the potential barrier governs the 3D oriented assembly in the later sections.

3.2. Mesoporous and Oriented Characteristics. Zinc oxide is an important semiconductive material with wide band gap, high thermal stability, and excellent catalysis activity.[35−39] Especially, ZnO with well-defined nanostructures shows high

dx.doi.org/10.1021/ic2009013 |*Inorg. Chem.* 2011, 50, 5841–5847

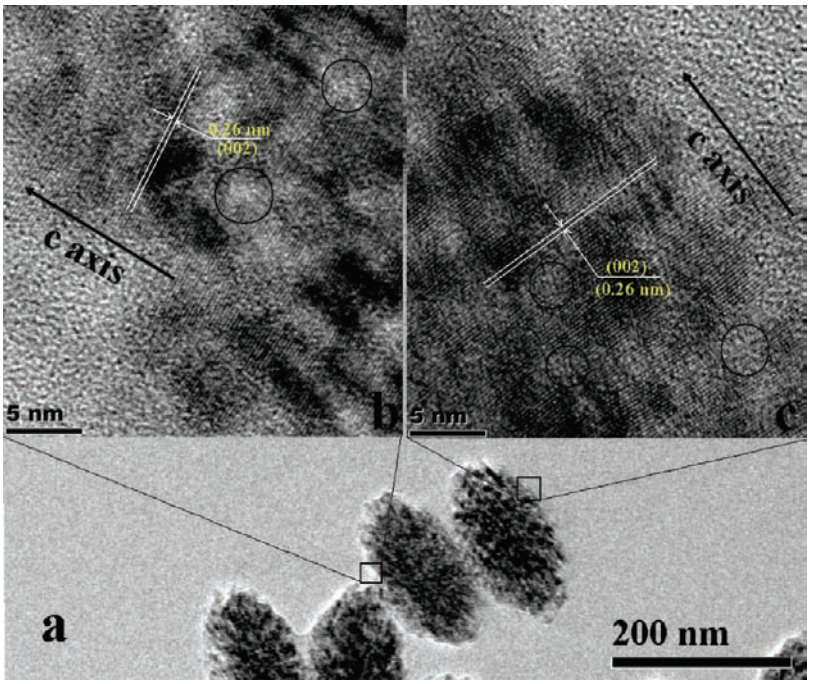

Figure 3. High-resolution TEM images. (a) TEM images of 190 × 111 nm ZnO mesoporous ellipsoids. (b, c) Corresponding high-resolution TEM images, in which the high crystallographic orientations perpendicular or parallel to *c* axis were clearly observed.

photocatalytic efficiency and can be cheaply obtained. A large number of ZnO nanostructures, such as wires, helices, belts, tubes, and sheets, have been successfully produced with more than one method.[40−44] However, the well-defined mesoporous structure of ZnO has rarely been reported. In the current paper, highly uniform ZnO mesoporous ellipsoids were directly assembled from ligand-free ZnO nanocrystals, of which the size can be tuned by adding various contrentration of hexane in the MDC solvent system (see Figure 2) or varying the size of primary ZnO nanocrystals (see Figure S2, Supporting Information). Figure 2 shows the TEM images of highly uniform ZnO mesoporous ellipsoids with a length-to-width ratio of ∼1.7, with average diameter of 5 nm (Figure S1a, Supporting Information). The mesoporous characteristics can even be observed from TEM images with higher magnification (such as Figure 2b,d,f). The size of uniform ZnO mesoporous ellipsoids can be slightly tuned between 190 × 111 and 175 × 101 nm by changing the concentration of hexane in the MDC solvent system.

The mesoporous nature of these uniform ZnO ellipsoids is confirmed by nitrogen physisorption (Figure S3, Supporting Information). The detected specific BET surface area of ZnO mesoporous ellipsoids with length × width of 190 × 111 nm is equal to 136.57 m^2/g, while their average BJH pore diameter is 8.8 nm. Compared to previously reported ZnO structures,[40−44] the higher specific BET surface area of ZnO ellipsoids is ascribed to the small particle size (5 nm) and high surface activity of ligand-free ZnO nanocrystal building blocks, since the measurement of nitrogen physisorption is highly dependent on the surface properties of nanostructures.[1−13]

OA has been considered to be one of most important mechanisms that govern the crystal growth in nanoscale regimes, which is obviously different from the classic kinetics of Ostwald ripening.[28] In the process of OA, crystallite particles aggregate irreversibly along high-energy crystallographic facets in a highly oriented manner, which is driven by the reduction of the surface energy of the whole system.[25−27,45,46] Regretfully, OA gives rise to homogeneous single crystals or 1D structures in most of the cases, since the preference of OA is usually unidirectional.[28,29] There are rarely works demonstrating the synthesis of 2D or even 3D quasisingle crystals by OA.[29] Very recently, Lou et al. achieved successfully the formation of 2D assemblies of hematite (α-Fe_2O_3) nanoparticles with diameter of 100 nm at a relatively low temperature of 105 °C by OA.[29] It was found that the hematite nanoparticle building blocks were attached to each other not only along the longitudinal axis but also the lateral direction with prolonged reaction, although the 1D chainlike structures are first formed by OA during the early stage of the reaction. From Lou et al.'s work,[29] we reach the conclusion that the 3D microstructures can also be assembled by OA, if the essential factors controlling the dynamics of 3D oriented assembly are properly addressed. Here, we show that the 3D ZnO nanostructures can be perfectly assembled by OA at room temperature, if the solvent for dispersing nanocrystal building blocks is suitably prepared.

Obviously, OA is addressed to be the governing mechanism for this 3D assembly from Figure 3, which shows that the uniform ZnO mesoporous ellipsoids had perfect crystallographic orientation along *c* axis, which confirmed directly the oriented assembly process of ZnO nanocrystal building blocks along the *c* axis. It is noted that ZnO nanocrystals attached with adjacent ones along orientations perpendicular to the *c* axis also by the OA mechanism, although some minor dislocations arose at the interfaces. As marked by black circles in Figure 3b,c, the mesoporous structures could be directly observed at the thin edges of a ZnO mesoporous ellipsoid. Moreover, the oriented characteristics were also confirmed by the analysis from XRD spectra. Comparing parts a and b of Figure S4 (Supporting Information), it can be observed that the diffraction peak of (002) and (100) of ZnO mesoporous

ellipsoids has become narrower than that in corresponding nanocrystals, which indicates the long-range oriented interactions among ZnO nanocrystal building blocks both parallel and perpendicular to the *c* axis.

3.3. Assembling Dynamics by OA. For the assembly under conditions of the absence of organic ligands, it is necessary to design a novel procedure for assembling ligand-free building blocks, since the nucleation and growth dynamics of ligand-free building blocks are obviously different from those depending on organic ligand.[20−24] Ganapathy et al.'s work enlightens us on designing a novel procedure where the 2D assembly of colloidal particles obeys the same nucleation and growth laws that govern atomic epitaxy growth, which implied that micrometer- and nanometer-scale particles could be employed as "artificial atoms" to assemble desired microstructures, if the nucleation and growth dynamics of these "artificial atoms" were efficiently controlled.[47] However, how to control the nucleation and growth dynamics of nanocrystal assembly is still challenging scientists.

In order to control the dynamic process of nanocrystal assembly, the key is to determine which factors affect it. On the basis of the latest theoretical investigation about nanocrystal growth dynamics by OA mechanism, it can be first determined that the viscosity of the solvent plays an important role for the assembly of nanocrystal building blocks. According to the kinetic model built by Xu et al., the growth rate of nanocrystal morphology evolution could be described as follows[26]

$$v_i = k_i[n][A]^{ai} \quad (1)$$

where v_i (i = 1, 2, and 3) is the growth rate, k_i the rate constant, [n] the nanocrystal concentration, [A] the reactant concentration. The subscripts 1, 2, and 3 represent three growth directions. This result indicates that the growth rate is highly dependent on the rate constants along different directions. By adapting Xu et al.'s description, the dependence of the growth rate on the viscosity of the solvent can be built by the form of eq 2:

$$v_i = \frac{N_A k_B T}{\mu_i\left(1+\frac{5}{2}\Phi\right)}[n][A]^{ai} \quad (2)$$

Equation 2 shows simply that the growth rate of nanocrystals under the conditions of particle coalescence is governed by the viscosity of the solvent. On the other hand, according to the dynamic theory of crystal growth, the morphology and size of 3D crystal particles predominantly depended on the growth rates along different directions. Then, it is reasonable to conclude that the morphology and size of the assembled microstructures from nanocrystal building blocks can be tuned by controlling the viscosity of the solvent.

As early as the 1980s, it was revealed that the potential barrier of the solvent affected remarkably the dynamic process of solutes, besides the viscosity.[48,49] For example, Sundström et al. reported that the solvent dependence of the relaxation rate in TPM molecules cannot be described as usually done by viscosity dependence only, since the theoretical analysis deviates too much from the experimental results if compensating for the contribution from the potential barrier is not taken into account.[48] Therefore, the potential barrier of the solvent is reasonably determined by us to be the second key factor governing the assembly of nanocrystal building blocks.

According to the oriented growth mechanism proposed by Ribeiro et al., the coalescence may occur when particles collide

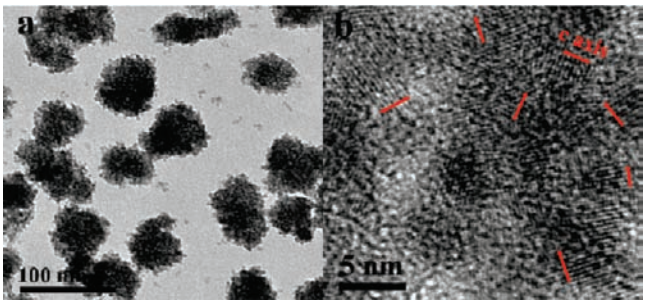

Figure 4. TEM images of ZnO agglomeration synthesized without adding diethyl carbonate: (a) low-resolution image and (b) high-resolution image showing the irregular agglomeration.

with similar crystallographic orientations.[27] In most cases, a nanocrystal particle has several kinds of crystal planes, in which the atomic density is different from each other. Does the probability of efficient collision, i.e., coalescence, taking place depend on the atomic density of crystal planes? Previous reports have confirmed the existence of this dependence.[26,27] When the building blocks are freely movable in the growth process, the rate constant can be written in the form of the Arrhenius equation:[26]

$$k_r = A_r \exp(-E/RT) \quad (3)$$

where E is the activation energy and R the gas constant. From the collision theory, the relation between rate constant k_r and atomic-density-dependent parameters Q_r and E can be built as follows:[27]

$$k_r = Q_r g(d_r, s_r) f(\varphi_r, T) \exp(-E/RT) \quad (4)$$

Equation 4 indicates that the rate constant is actually dependent on the properties of crystallographic facets of nanocrystals. Considering the consistency between the rate constant and the efficient collision probability, it can be easily inferred that the efficient collision probability is practically related to the crystallographic orientation. In most cases of oriented assembly, the efficient collision probability along the *c* axis of ZnO nanocrystals is higher than those perpendicular to the *c* axis, so that the 1D structure is usually produced with (001) orientation.[28,29,33,34] For the assembly of uniform ZnO mesoporous ellipsoids, a considerable potential barrier was created by introducing diethyl carbonate in the solvent system, which would change undoubtedly the collision degree. We suggest that the change in collision degree obviously will decrease the efficient collision probability along the *c* axis of ZnO, while this influence is negligible along crystallographic orientations with low efficient collision probability. As a result, the efficient collision probability perpendicular to the *c* axis is close to that along the *c* axis, which leads to the formation of 3D ZnO structures.

The above demonstration is in good agreement with previous reports[28,29,33,34] and our experimental results (Figure 4). In order to illustrate the influence of diethyl carbonate in oriented assembly of ZnO mesoporous ellipsoids, ZnO nanocrystals dispersed in the solvent without diethyl carbonate were also aged for the same time as that in the MDC solvent system. Figure 4a shows that ZnO microstuctures aged in the solvent without diethyl carbonate have irregular morphology and nonuniform size. Especially, it was observed from the high-resolution TEM image in Figure 4b that ZnO nanocrystals in the solvent without diethyl carbonate actually underwent an agglomerating

dx.doi.org/10.1021/ic2009013 |*Inorg. Chem.* 2011, 50, 5841–5847

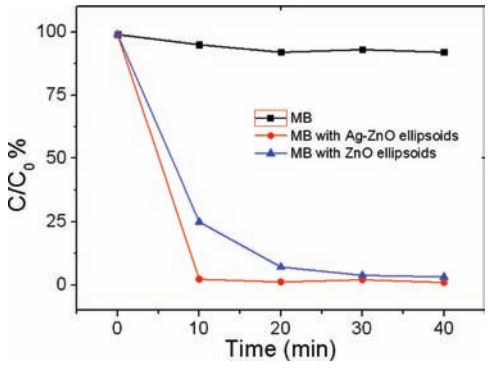

Figure 5. Photodegradation of MB by the as-synthesized ZnO mesoporous ellipsoids or Ag/ZnO mesoporous ellipsoid heterostructures under weak UV irradiation (2.1 mW/cm^2).

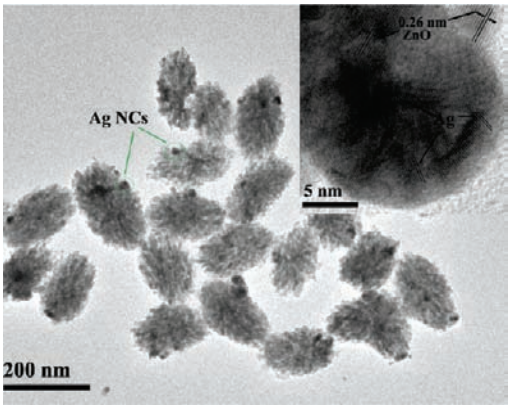

Figure 6. TEM images of Ag nanocrystals/ZnO mesoporous ellipsoid heterostructures (inset: the high-resolution TEM image of a Ag nanoparticle in the surface of a ZnO mesoporous ellipsoids).

process, which confirmed directly the importance of controlling the viscosity and potential barrier in the solvent system.

3.4. Photocatalysis. Recently, environmental pollution has become a problem not only in daily life of human beings but also other biological regimes.[50−52] Among the possible methods for degrading environmental pollutants, photocatalysis may be an idea that can be driven by the inexhaustible sunlight.[46] The excellent photocatalytic activity of ZnO has been confirmed and widely investigated in many works.[50,51,53] Besides the excellent photocatalytic activity, the cheapness and environmental sustainability of ZnO are also very attractive relative to other oxide catalysts. The efficient photocatalysis occurred primarily with the irradiation of ultraviolet, although some reports indicated that the irradiation could be extended into visible light range.[52] In order to achieve the photocatalytic degradation under sunlight, the photocatalytic activity of the applied catalyst should be high enough, since the power density of the UV portion of sunlight is very weak relative to that of many artificial UV light sources. For uniform ZnO mesoporous ellipsoids, the photocatalytic degradation of MB was carried out under weak UV irradiation (365 nm, 2.1 mW/cm^2). Figure 5 showed that the concentration of MB could decrease to 25% of the total after irradiation for 10 min.

Many recent reports confirmed that the heterostructures composed of noble metal and semiconductor nanocrystals showed higher catalytic activity than single semiconductor catalyst.[51] Therefore, we try to improve the catalytic activity of uniform ZnO mesoporous ellipsoids by assembling Ag nanocrystals into them. Figure 6 indicated clearly that Ag nanocrystals with an average diameter of 18 nm were encased homogeneously on the surfaces of uniform ZnO mesoporous ellipsoids. It was observed in Figure 5 that the photocatalytic activity of this heterostructure was remarkably enhanced so that the complete degradation of MB was finished in only 10 min, which opened a prospective method for weak UV photocatalysis based on ZnO materials.

4. SUMMARY

In conclusion, highly uniform ZnO mesoporous ellipsoids, in the scale between 132 × 75 to 190 × 111 nm (length × width), were directly assembled from ligand-free ZnO nanocrystal building blocks of ∼5 nm by the OA mechanism, in which the high surface activity of ligand-free nanocrystals were well-resolved and confirmed by the excellent photocatalytic activity under weak UV irradiation. Although the preference of OA is usually unidirectional, our investigations show that the uniform ZnO mesoporous ellipsoids have high crystallographic orientations both parallel and perpendicular to the *c* axis, which indicates that the 3D oriented assembly can be readily achieved, if the viscosity and potential barriers of the solvent system are properly controlled. These results open up an original possible way for both constructing directly the mesoporous structures from ligand-free nanocrystal building blocks and assembling 3D nanostructures by OA. We also believe that the highly uniform ZnO mesoporous ellipsoids, with high specific surface area and well-reserved surface activity from ligand-free nanocrystals, will supply the catalytic industries with a kind of highly efficient and cheap catalyst or catalyst support.

■ ASSOCIATED CONTENT

Supporting Information. Additional information as discussed in the text. This material is available free of charge via the Internet at http://pubs.acs.org.

■ AUTHOR INFORMATION

Corresponding Author

*E-mail: pengqing@mail.tsinghua.edu.cn.

■ ACKNOWLEDGMENT

This work was supported by the State Key Project of Fundamental Research for Nanoscience and Nanotechnology (2011CB932401, 2011CBA00500) and the Foundation for Innovative Research Groups of the National Natural Science Foundation of China (Grant No. 20921001).

■ REFERENCES

(1) Kresge, C. T.; Leonowicz, M. E.; Roth, W. J.; Vartuli, J. C.; Beck, J. S. *Nature* **1992**, *359*, 710–712.

(2) Beck, J. S.; Vartuli, J. C.; Roth, W. J.; Leonowicz, M. E.; Kresge, C. T.; Schmitt, K. D.; Chu, C. T. W.; Olson, D. H.; Sheppard, E. W. *J. Am. Chem. Soc.* **1992**, *114*, 10834–10843.

(3) Li, H. X.; Bian, Z. F.; Zhu, J.; Zhang, D. Q.; Li, G. S.; Huo, Y. N.; Li, H.; Lu, Y. F. *J. Am. Chem. Soc.* **2007**, *129*, 8406–8407.

(4) Zhu, Y.; Shi, J.; Shen, W.; Dong, X.; Feng, J.; Ruan, M.; Li, Y. *Angew. Chem., Int. Ed.* **2005**, *44*, 5083–5087.

(5) Zürner1, A.; Kirstein1, J.; Döblinger1, M.; Bräuchle1, C.; Bein, T. *Nature* **2007**, *450*, 705–708.
(6) Walcaarius, A.; Sibotter, E.; Eeienne, M.; Ghanbaja, J. *Nat. Mater.* **2007**, *6*, 602–608.
(7) Orosco, M. M.; Pacholski, C.; Sailor, M. J. *Nat. Nanotechnol.* **2009**, *4*, 225–228.
(8) Armatas, G. S.; Kanatzidis, M. G. *Science* **2006**, *313*, 817–820.
(9) Monnier, A.; Schüth, F.; Huo, Q.; Kumar, D.; Margolese, D.; Maxwell, R. S.; Stucky, G.; Krishnamurty, M.; Petroff, P.; Firouzi, A.; Janicke, M.; Chmelka, B. *Science* **1993**, *261*, 1299–1303.
(10) Huo, Q.; Margolese, D.; Ciesla, U.; Demuth, D. G.; Feng, P.; Gier, T. E.; Sieger, P.; Firouzi, A.; Chmelka, B. F. *Chem. Mater.* **1994**, *368*, 1176–1191.
(11) Attard, G. S.; Glyde, J. C.; Göltner, C. G. *Nature* **1995**, *378*, 366–368.
(12) Zhao, D.; Feng, J.; Huo, Q.; Melosh, N.; Fredrickson, G. H.; Chmelka, B. F.; Stucky, G. D. *Science* **1998**, *279*, 548–552.
(13) Lu, A. H.; Schmidt, W.; Taguchi, A.; Spliethoff, B.; Tesche, B.; Schüth, F. *Angew. Chem., Int. Ed.* **2002**, *41*, 3489–3492.
(14) Joo, S. H.; Park, J. Y.; Tsung, C. K.; Yamada, Y.; Yang, P. D.; Somorjai, G. A. *Nat. Mater.* **2009**, *8*, 126–131.
(15) Zhuang, J. Q.; Wu, H. M.; Yang, Y. G.; Cao., Y. C. *Angew. Chem., Int. Ed.* **2008**, *47*, 2208–2212.
(16) Zhuang, J.; Wu, H.; Yang, Y.; Cao, Y. C. *J. Am. Chem. Soc.* **2007**, *129*, 14166–14167.
(17) Russell, V. A.; Evans, C. C.; Li, W. J.; Ward, M. D. *Science* **1997**, *276*, 575–579.
(18) Eddaoudi, M.; Kim, J.; Rosi, N.; Vodak, D.; Wachter, J.; O'Keeffe, M.; Yaghi, O. M. *Science* **2002**, *295*, 469–472.
(19) El-Kaderi, H. M.; Hunt, J. R.; Mendoza-Cortes, J. L.; Cote, A. P.; Taylor, R. E.; O'Keeffe, M.; Yaghi, O. M. *Science* **2007**, *316*, 268–272.
(20) Bai, F.; Wang, D. S.; Huo, Z. Y.; Chen, W.; Liu, L. P.; Liang, X.; Chen, C.; Wang, X.; Peng, Q.; Li, Y. D. A *Angew. Chem., Int. Ed.* **2007**, *46*, 6650–6653.
(21) Wang, L. Y.; Li, P.; Zhuang, J.; Bai, F.; Feng, J.; Yan, X. Y.; Li, Y. D. *Angew. Chem., Int. Ed.* **2008**, *47*, 1054–1057.
(22) Wang, D. S.; Xie, T.; Peng, Q.; Li, Y. D. *J. Am. Chem. Soc.* **2008**, *130*, 4016–4022.
(23) Li, P.; Peng, Q.; Li, Y. D. *Adv. Mater.* **2009**, *21*, 1945–1948.
(24) Chen, C.; Nan, C. Y.; Wang, D. S.; Su, Q.; Duan, H. H.; Liu, X. W.; Zhang, L. S.; Chu, D. R.; Song, W. G.; Peng, Q.; Li, Y. D. *Angew. Chem., Int. Ed.* **2011**, *50*, 1–6.
(25) Pacholski, C.; Kornowski, A.; Weller, H. *Angew. Chem., Int. Ed.* **2002**, *41*, 1188–1191.
(26) Xu, X.; Liu, F.; Yu, K.; Huang, W.; Peng, B.; Wei, W. *ChemPhysChem* **2007**, *8*, 703–711.
(27) Ribeiro, C.; Lee, E. J. H.; Longo, E.; Leite, E. R. *ChemPhysChem* **2005**, *6*, 690–696.
(28) Mallavajula, R. K.; Archer, L. A. *Angew. Chem., Int. Ed.* **2011**, *50*, 578–580.
(29) Chen, J.; Zhu, T.; Li, C.; Lou, X. *Angew. Chem., Int. Ed.* **2011**, *50*, 650–653.
(30) Zhang, Z.; Sun, H.; Shao, X.; Li, D.; Yu, H.; Han, M. *Adv. Mater.* **2005**, *17*, 42–47.
(31) Xu, H.; Wang, W.; Zhu, W.; Zhou, L.; Ruan, M. *Cryst. Growth Des.* **2007**, *7*, 2720–2724.
(32) Liu, J.; Huang, X.; Li, Y.; Sulieman, K.; He, X.; Sun, F. *Cryst. Growth Des.* **2006**, *6*, 1690–1696.
(33) Yu, J.; Joo, J.; Park, H.; Baik, S.; Kim, Y.; Kim, S.; Hyeon, T. *J. Am. Chem. Soc.* **2005**, *127*, 5662–5670.
(34) Pradhan, N.; Xu, H.; Peng, X. *Nano Lett.* **2006**, *6*, 720–724.
(35) Huang, M. H.; Mao, S.; Feick, H.; Yan, H.; Wu, Y.; Kind, H.; Weber, E.; Russo, R.; Yang, P. *Science* **2001**, *292*, 1897–1899.
(36) Pan, Z. W.; Dai, Z. R.; Wang, Z. L. *Science* **2001**, *291*, 1847–1849.
(37) Lin, D.; Wu, H.; Zhang, R.; Pan, W. *Chem. Mater.* **2009**, *21*, 3479–3484.
(38) Sharma, P.; Gupta, A.; Rao, K. V.; Owens, F. J.; Sharma, R.; Ahuja, R.; Guillen, J. M.; Johansson, B.; Gehring, G. A. *Nat. Mater.* **2003**, *2*, 673–677.
(39) Law, M.; Greene, L.; Johnson, J. C.; Saykally, R.; Yang, P. D. *Nat. Mater.* **2005**, *4*, 455–459.
(40) Park, W. I.; Yi, G. C. *Adv. Mater.* **2004**, *16*, 87–90.
(41) Zhao, M. H.; Wang, Z. L.; Mao, S. X. *Nano Lett.* **2004**, *4*, 587–590.
(42) Tian, Z. R.; Voigt, J. A.; Liu, J.; Mckenzie, B.; Mcdermott, M. J.; Rodriguez, M. A.; Konishi, H.; Xu, H. *Nat. Mater.* **2003**, *2*, 821–826.
(43) Hu, J. Q.; Li, Q.; Meng, X. M.; Lee, C. S.; Lee, S. T. *Chem. Mater.* **2003**, *15*, 305–308.
(44) Hu, J. Q.; Bando, Y.; Zhan, J. H.; Li, Y. B.; Sekiguchi, T. *Appl. Phys. Lett.* **2003**, *83*, 4414.
(45) Zitoun, D.; Pinna, N.; Frolet, N.; Belin, C. *J. Am. Chem. Soc.* **2005**, *127*, 15034–15035.
(46) Nguyen, T.; Do., T. *J. Phys. Chem. C* **2009**, *113*, 11204–11214.
(47) Ganapathy, R.; Buckley, M. R.; Gerbode, S. J.; Cohen, I. *Science* **2010**, *327*, 445–448.
(48) Sundström, V.; Gillbro, T. *J. Chem. Phys.* **1984**, *81*, 3463–3474.
(49) Hicks, J.; Vandersall, M.; Babarogic, Z.; Eisenthal, K. B. *Chem. Phys. Lett.* **1985**, *116*, 18–24.
(50) Awazu, K.; Fujimaki, M.; Rockstuhl, C.; Tominaga, J.; Murakami, H.; Ohki, Y.; Yoshida, N.; Watanabe, T. A. *J. Am. Chem. Soc.* **2008**, *130*, 1676–1680.
(51) Zheng, Y.; Zheng, L.; Zhan, Y.; Lin, X.; Zheng, Q.; Wei, K. *Inorg. Chem.* **2007**, *46*, 6980–6986.
(52) Asahi, R.; Morikawa, T.; Ohwaki, T.; Aoki, K.; Taga, Y. *Science* **2001**, *293*, 269–271.
(53) Yang, J. L.; An, S. J.; Park, W. I.; Yi, G. C.; Choi, W. *Adv. Mater.* **2004**, *16*, 1661–1664.